Non-thermal plasma etching of MOF thin films in high optical quality for interference sensing

Pavel Alekseevskiy, Maria Timofeeva, Semyon Bachinin, Regis Peignier, Cedric Noel, Pascal Boulet, Thierry Belmonte, Valentin Milichko

▶ **To cite this version:**

Pavel Alekseevskiy, Maria Timofeeva, Semyon Bachinin, Regis Peignier, Cedric Noel, et al.. Non-thermal plasma etching of MOF thin films in high optical quality for interference sensing. Optical Materials, 2025, 154, pp.115666. ⟨10.1016/j.optmat.2024.115666⟩. ⟨hal-04717875⟩

HAL Id: hal-04717875

https://hal.univ-lorraine.fr/hal-04717875v1

Submitted on 2 Oct 2024

HAL is a multi-disciplinary open access archive for the deposit and dissemination of scientific research documents, whether they are published or not. The documents may come from teaching and research institutions in France or abroad, or from public or private research centers.

L'archive ouverte pluridisciplinaire **HAL**, est destinée au dépôt et à la diffusion de documents scientifiques de niveau recherche, publiés ou non, émanant des établissements d'enseignement et de recherche français ou étrangers, des laboratoires publics ou privés.

Distributed under a Creative Commons CC BY 4.0 - Attribution - International License

Non-thermal plasma etching of MOF thin films in high optical quality for interference sensing☆

Pavel V. Alekseevskiy [a], Maria Timofeeva [a], Semyon Bachinin [a], Regis Peignier [b], Cedric Noel [b], Pascal Boulet [b], Thierry Belmonte [b], Valentin A. Milichko [a,b,*]

[a] School of Physics and Engineering, ITMO University, St. Petersburg, 197101, Russia
[b] Universite de Lorraine, CNRS, IJL, Nancy, F-54000, France

ABSTRACT

Metal–organic frameworks (MOFs) in a thin film (TF) form have appeared recently as multifunctional elements for micro- and opto-electronic devices. However, achieving the roughness of MOF TF less than 10 nm is still a challenge, which limits their further integration with the corresponding devices. Here, we report on plasma etching (PE) approach allowing one to improve the quality of MOF TF surfaces. We demonstrate that PE of a spin-coated HKUST-1 TFs with a varied thickness (1.9 to 3 μm) and roughness (more than 200 nm) decreases the film roughness by 100 times (up to 2 nm), while the chemical composition and the structure remain. As a result, an optical quality for the TF surface can be achieved resulting to a mirror like reflectivity as well as an optical sensitivity of water through the interference effect. The obtained results, thereby, pave the way to a universal post-processing of MOF TFs for diverse applications where their roughness plays a key role.

1. Introduction

Metal–organic frameworks (MOFs) are a wide class of artificial hybrid materials based on metallic nodes and organic ligands, linked together with different chemical bonds [1]. Possessing a high level of porosity and organic–inorganic nature, MOFs can be utilized for diverse applications, such as gas sorption and filtration, catalysis, water harvesting, bio and optical sensing, optical switching, data storage and optoelectronics in general [2–4]. Thanks to the development of modern reticular chemistry, functional MOFs can be scaled now from the powder or single crystal to a thin film (TF) form, which paves the way an industrial application of MOFs [5–7]. Indeed, existing approaches of MOF TF fabrication such as spin-coating (SC), layer by layer (LB), chemical vapour deposition (CVD) etc. provide large scale and high quality (in terms of crystallinity and composition) films of a varied thickness and morphology [8–10]. Moreover, the obtained MOF TFs are usually utilized as nonlinear optical materials for light manipulation and limiting [11–13]. However, achieving the roughness of MOF TF less than 10 nm is still a challenge, which limits their further integration with opto- and micro-electronic devices [14].

Here, we made an assumption that the combination of a common TF fabrication approach like SC with an industry-oriented post-processing may overcome this challenge. As the latter, we can consider a non-thermal plasma (NTP) providing a well-known efficient, and fast surface treatment (via activation [15], cleaning [16,17], functionalization [18], and plasma etching (PE) [19]). Being a non-equilibrium cold atmospheric pressure plasma, NTP is characterized by an electron (10^4–10^5 K) and a gas temperature close to a room one (up to few hundreds Kelvin) [20,21]. Therefore, the NTP treatment proceeds by the reactive species, appeared through the collision of electrons and gas molecules [22]. Herein, a non-equilibrium character of the NTP provides a gentle treatment of TFs, and hence could be considered as a promising post-processing for MOFs [23–26].

Using such an approach, we demonstrate that the plasma etching of a spin-coated HKUST-1 thin films (PESC HKUST-1 TFs) with a varied thickness (1.9 to 3 μm) and roughness (more than 200 nm) decreases the film roughness by 100 times (up to 2 nm, Fig. 1), while the chemical composition and the structure remain. As a result, an optical quality [27] for the MOF TF surface can be achieved resulting to a mirror like reflectivity as well as an optical sensitivity of water through the interference effect. The obtained results, thereby, pave the way to a universal post-processing of MOF TFs for diverse applications where their roughness plays a key role.

☆ This research project funded by the Russian Science Foundation (Grant №23-22-00285).
* Corresponding author at: School of Physics and Engineering, ITMO University, St. Petersburg, 197101, Russia.
E-mail addresses: thierry.belmonte@univ-lorraine.fr (T. Belmonte), v.milichko@metalab.ifmo.ru (V.A. Milichko).

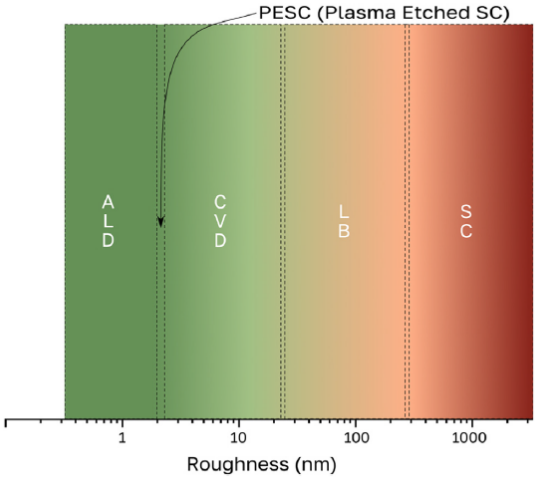

Fig. 1. Roughness of MOF TFs, obtained by chemical vapour deposition (CVD), layer by layer (LB), spic-coating (SC), and proposed PESC (plasma etching coupled with the spin coating) approach. Atomic layer deposition (ALD) is for comparison.

2. Experimental section

2.1. MOF thin film fabrication

As a model MOF for thin film fabrication and plasma etching, HKUST-1 has been selected [28]. To synthesize it, 15 mg of copper(II) acetate hydrate ($Cu(AcO)_2H_2O$) and 31.5 mg of benzene-1,3,5-tricarboxylic acid (BTC) as a ligand have been individually mixed in 50 mL of ethanol followed by stirring in an ultrasonic bath for 10 min at room temperature. Then, each solution has been stored in syringes, placed on an automated SC system to fabricate MOF TFs (Fig. 2a). As a film substrate, fused silica (18 × 18 mm) has been utilized. Prior to the TF fabrication, the substrate has been purified in isopropyl alcohol in an ultrasonic bath for 10 min followed by O_2 plasma treatment. The substrate has been glued to the SC plate with an adhesive tape (Fig. 2a). The following parameters for TF fabrication have been set at 880 rpm, 400 and 600 synthesis cycles with no heating. As a result, the HKUST-1 TFs have been successfully obtained.

2.2. Plasma etching

For the plasma etching, an argon plasma jet has been produced by a microwave surfatron applicator operating at atmospheric pressure. Microwave power has been delivered by a 2.45 GHz solid-state microwave generator, while the plasma absorbed power has been set to 25 W. A fused silica tube (6 mm inner diameter) has been inserted inside the microwave cavity. The microwave plasma has been generated inside this tube where a 225 sccm (standard cubic centimeter per min) argon gas flow has been injected through a mass flow meter. The tube has been bended, so that an angle of 40° is formed between its axis and the HKUST-1 TF surface. Experimental scheme of corresponding PE during 3 to 7 min (Figures S3-S5) of HKUST-1 TFs is presented in Fig. 2b.

2.3. Structural characterization

X-ray diffraction (XRD) measurements have been performed on a D8 Bruker AXS diffractometer in a $\theta/2\theta$ configuration, equipped with a Ge(111) Johansson monochromator on a primary side and a Lynxeye

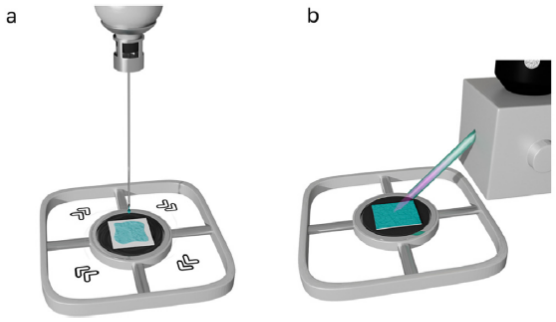

Fig. 2. (a) Scheme of spin-coating (SC), (b) and plasma etching (PE) post-processing of MOF TF.

Position Sensitive detector. Samples have been allowed to rotate at 15 rpm during the scan which have been taken with a step size of 0.021° in 2θ with 2 s/step.

The atomic-force microscopy (AFM) have been done by the Smart-SPM 1000 (AIST-NT microscope) in semi-contact mode at ambient conditions. Working cantilevers was HQ:NSC16/Hard/Al BS (Mikro-Masch) with 190 kHz resonant working frequency and 45 N m^{-1} force constant.

The scanning electron microscopy (SEM) has been performed with FEI Quanta Inspect S in high resolution mode by large-field detector (LFD) at 2000x and 20 kV accelerating voltage.

2.4. Optical characterization

Optical transmission, reflection and optical sensing for HKUST-1 TFs have been measured using the confocal microspectroscopy setup (see Figure S1) at ambient condition [29]. For the transmission, the MOF TFs have been irradiated with a white light source (halogen lamp HL-2000 FHSA Ocean Optics) through 10x/0.26 NA objective (Mitutoyo M Plan APO NIR); while the transmission and reflection signals have been collected via 50x/0.42 NA objective (Mitutoyo M Plan APO NIR), and then analyzed using confocal Raman Spectroscopy system (HORIBA Labram, 150 g mm^{-1} diffraction grating and water-cooling camera ANDOR DU 420 A - OE 325 CCD). For the optical sensing, the MOF TFs have been irradiated with 1050 nm Yb^{3+} laser (TeMa, Avesta Project, 150 fs pulse duration, 80 MHz repetition rate) via 10x/0.26 NA objective (Mitutoyo M Plan APO NIR) and with a white light source simultaneously. Confocal Raman spectroscopy has been also performed for HKUST-1 TFs with 632.8 nm He-Ne continuous laser radiation (15 mW) in reflection mode through 50x/0.42 NA objective. The collecting signal has been analyzed by Horiba Labram Spectrometer with 600 g mm^{-1} diffraction grating and water-cooling ANDOR camera (DU 420 A - OE 325 CCD).

3. Results and discussion

As can be seen in Fig. 3a an optical image of as-synthesized HKUST-1 TFs shows a homogeneous surface with a characteristic blue color of HKUST-1 [30] which scatters the light diffusely. After the PE, the surface of the HKUST-1 TFs changes significantly (see Fig. 3b and Figures S2-S5): First, the unique interference patterns on the surface and the mirror like reflectivity appeared; second, the domain structure of the HKUST-1 TFs reveals itself with an average size of 96 μm.

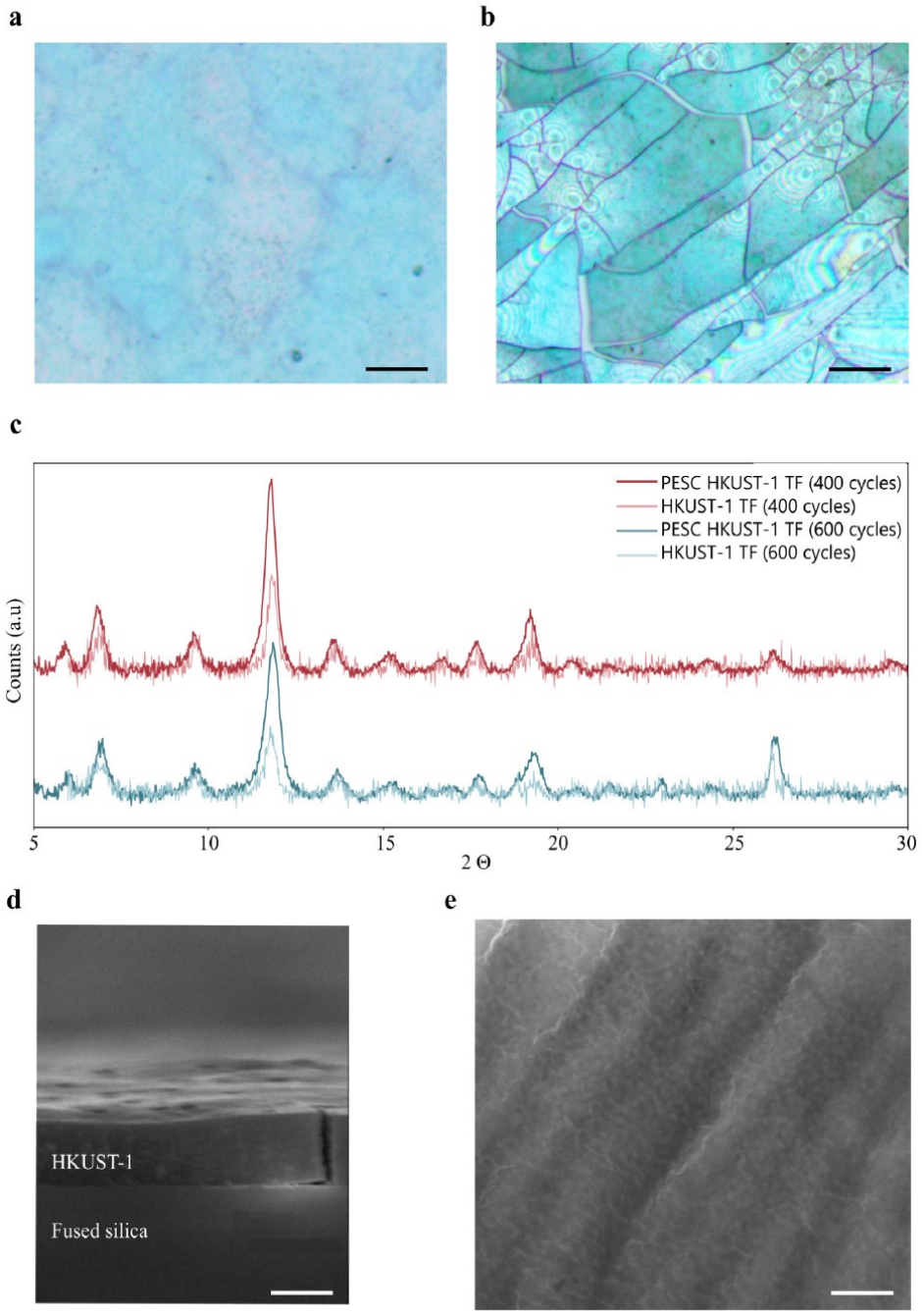

Fig. 3. Optical images of as-synthesized HKUST-1 TF (a) and PESC HKUST-1 TFs (b). Scale bars, 100 μm. (c) X-ray diffraction patterns of as-synthesized and PESC HKUST-1 TFs. (d) SEM cross-section of the as-synthesized HKUST-1 TF and (e) SEM micrograph of PESC HKUST-1 TF. Scale bars, 20 μm (d), 3 μm (e).

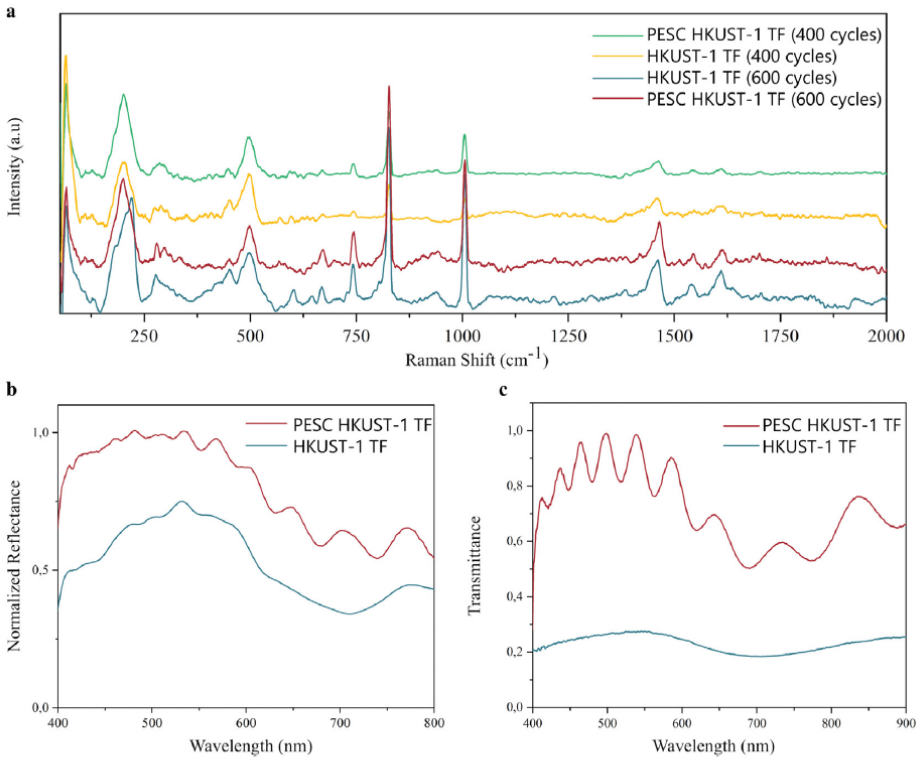

Fig. 4. (a) Raman spectra for as-synthesized and PESC HKUST-1 TFs. (b) Normalized reflectance and (c) transmittance spectra for as-synthesized and PESC HKUST-1 TFs.

The XRD analysis demonstrates that the diffraction patterns of the PESC HKUST-1 TFs and as-synthesized HKUST-1 TFs are similar (Fig. 3c): the position of the diffraction peaks for both TFs preserved, the parameters of which allowed us to estimate an average side of domains (23 nm for as-synthesized HKUST-1 TF and 21 nm for PESC HKUST-1 TF, see Table S1); while the intensity of the peaks for PESC HKUST-1 TF increased with a slight decreasing of their width and noise level (Figures S6-S8). Energy dispersive X-ray (EDX) analysis also revealed the uniform distribution of elements over the surface of HKUST-1 TF during the PE (Figure S13). Similar results have been also obtained by confocal Raman spectroscopy. As one can see in Fig. 4a, the Raman spectra of the as-synthesized HKUST-1 TF and PESC HKUST-1 TF demonstrate the characteristic Cu–Cu bond (50 to 200 cm^{-1}), coordination bond Cu–Ox (200 up to 700 cm^{-1}), and fingerprint BTC ligand vibrations (C-H at 750 and 900 cm^{-1}, C=C at 1000 cm^{-1}, C-O-O at 1485 cm^{-1} and C-O at 1550–1600 cm^{-1}) [31]. According to XRD, EDS, and Raman analysis we concluded that the PE be considered as a non-damaging post-processing of HKUST-1 TFs.

Considering that the chemical mechanism is the most possible for HKUST-1 TH etching (see SI and Figure S14), leading to improved surface quality [19], we have performed an analysis of the HKUST-1 TF surfaces. SEM micrographs and corresponding cross-section of the as-synthesized HKUST-1 TFs and PESC HKUST-1 TF (Fig. 3d,e) demonstrate a homogeneous and flat surface with the thickness varied from 1.9 to 3 μm (according to the synthesis cycles). However, comparative analysis of the surface by AFM revealed that the average roughness of the as-synthesized HKUST-1 TF is 200 nm (Fig. 5a,c, and Figures S9-S11); while the PE of the surface reduces the roughness by 2 orders of magnitude (up to 2 nm, see Fig. 5b,d). This statement has been also confirmed by optical profilometry, showing a high degree of homogeneity of the PESC HKUST-1 TF (Figure S12). The latter results bring us to an idea that PESC HKUST-1 TF surface can be characterized with an optical quality [27].

Therefore, we have performed the optical reflectance and transmittance analysis by confocal optical setup. As one can see in Fig. 4b,c, the reflectance of the PESC HKUST-1 TFs has been increased by 30% compared to as-synthesized HKUST-1 TFs; while the transmission has been improved by 5 times due to suppressed diffusion scattering of light. Herein, characteristic interference pattern appeared for the PESC HKUST-1 TF in reflectance and transmittance regimes (Fig. 4b,c). We have also analyzed the fringe visibility of this interference, which is equal to 0.11, while no interference has been detected for the as-synthesized HKUST-1 TFs. Important is that the indication of this characteristic interference pattern for smooth PESC HKUST-1 TFs opens up the possibility to create MOF-based TF sensors or micro- and opto-electronic elements where the roughness plays a crucial role [32, 33].

To confirm this, we refer to the work [34] demonstrating that the single crystals of HKUST-1 can be optically switched (color change) by laser and returned to initial state by absorbing H_2O molecules from the ambient. Based on this, we have realized an optical interference sensor of water based on PESC HKUST-1 TF. Fig. 6a demonstrates the transmittance spectra of the PESC HKUST-1 TF at ambient condition upon the action of the laser irradiation (1050 nm): no any changes can be detected, since H_2O has been removed by heating during the PE processing of HKUST-1 TF (dried). However, as soon as water

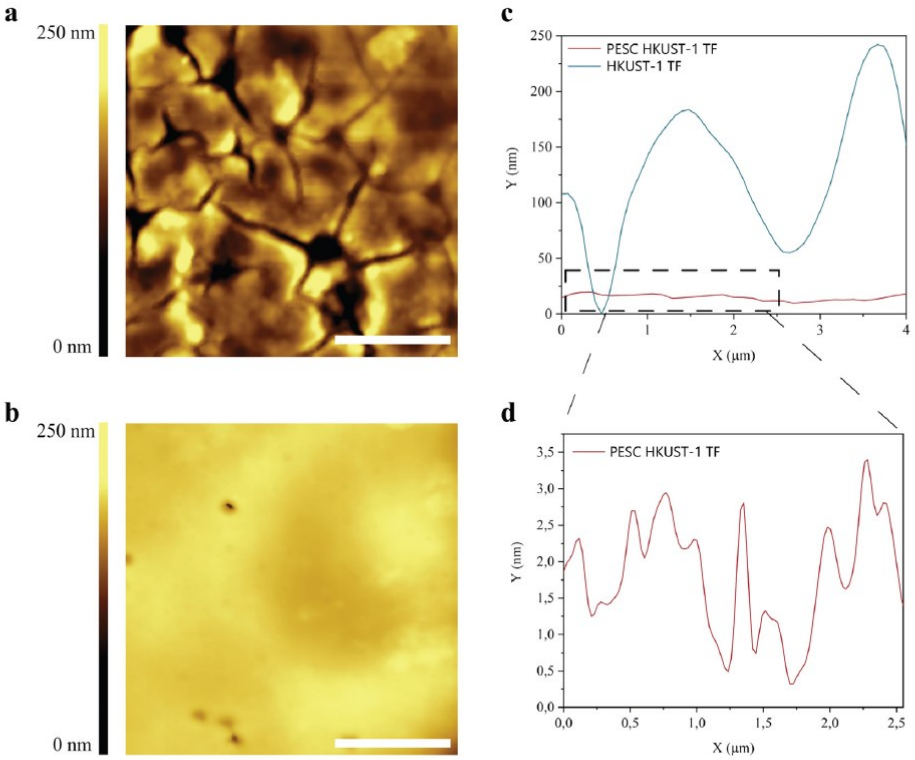

Fig. 5. AFM characterization of as-synthesized (a) and PESC HKUST-1 TFs (b-d). Comparison of TF roughness for as-synthesized and PESC HKUST-1 TFs in (c). Scale bars, 5 μm (a,b).

vapor is applied (PESC HKUST-1 TF (wet) in Fig. 6b), the reversible optical switching (15 nm shift of the interference) can be detected, corresponding to the interaction between guest (H_2O) molecules and the framework [35].

4. Conclusion

In summary, we report on plasma etching approach allowing one to improve the quality of MOF thin film surfaces. In details, we demonstrate that the plasma etching of a spin-coated HKUST-1 thin films with a varied thickness (1.9 to 3 μm) and roughness (more than 200 nm) decreases the film roughness by 100 times (up to 2 nm), while the chemical composition and the structure remain. As a result, an optical quality for the film surface can be achieved, resulting to a mirror like reflectivity as well as an optical sensitivity of water through the interference effect. The obtained results, thereby, pave the way to a universal post-processing of MOF thin films for diverse applications where their roughness plays a key role.

Acknowledgments

P.V.A acknowledges the financial support of the Russian Science Foundation (Grant № 23-22-00285). The authors acknowledge Dr. A. Krasilin for supporting in SEM analysis.

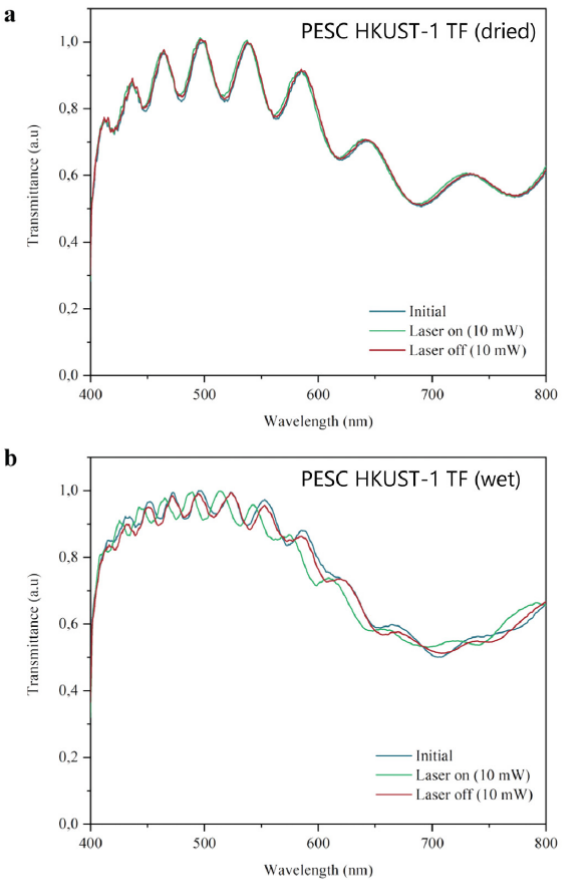

Fig. 6. Normalized transmittance spectra for PESC HKUST-1 TF upon the action of the laser radiation (1050 nm wavelength, 10 mW integral power): (a) HKUST-1 TF, obtained by the PE and corresponding to a dry state, and (b) as soon as water vapor is applied to PECS HKUST-1 TF (i.e., wet) demonstrating reversible 15 nm spectral shift of the interference pattern.

References

[1] H.-C. Zhou, J.R. Long, O.M. Yaghi, Introduction to metal–organic frameworks, Chem. Rev. 112 (2) (2012) 673–674, http://dx.doi.org/10.1021/cr300014x.

[2] Y.A. Mezenov, A.A. Krasilin, V.P. Dzyuba, A. Nominé, V.A. Milichko, Metal–organic frameworks in modern physics: Highlights and perspectives, Adv. Sci. 6 (17) (2019) 1900506, http://dx.doi.org/10.1002/advs.201900506.

[3] N. Kulachenkov, Q. Haar, S. Shipilovskikh, A. Yankin, J.-F. Pierson, A. Nominé, V.A. Milichko, MOF-based sustainable memory devices, Adv. Funct. Mater. 32 (5) (2022) 2107949, http://dx.doi.org/10.1002/adfm.202107949.

[4] I. Stassen, N. Burtch, A. Talin, P. Falcaro, M. Allendorf, R. Ameloot, An updated roadmap for the integration of metal–organic frameworks with electronic devices and chemical sensors, Chem. Soc. Rev. 46 (11) (2017) 3185–3241, http://dx.doi.org/10.1039/C7CS00122C.

[5] L. Heinke, C. Wöll, Surface-mounted metal–organic frameworks: Crystalline and porous molecular assemblies for fundamental insights and advanced applications, Adv. Mater. 31 (26) (2019) 1806324, http://dx.doi.org/10.1002/adma.201806324.

[6] C. Crivello, S. Sevim, O. Graniel, C. Franco, S. Pané, J. Puigmartí-Luis, D. Muñoz-Rojas, Advanced technologies for the fabrication of MOF thin films, Mater. Horiz. 8 (1) (2021) 168–178, http://dx.doi.org/10.1039/D0MH00898B.

[7] O. Shekhah, J. Liu, R.A. Fischer, C. Wöll, MOF thin films: existing and future applications, Chem. Soc. Rev. 40 (2) (2011) 1081–1106, http://dx.doi.org/10.1039/C0CS00147C.

[8] V. Chernikova, O. Shekhah, M. Eddaoudi, Advanced fabrication method for the preparation of MOF thin films: Liquid-phase epitaxy approach meets spin coating method, ACS Appl. Mater. Interfaces 8 (31) (2016) 20459–20464, http://dx.doi.org/10.1021/acsami.6b04701.

[9] I. Stassen, M. Styles, G. Grenci, H.V. Gorp, W. Vanderlinden, S.D. Feyter, P. Falcaro, D.D. Vos, P. Vereecken, R. Ameloot, Chemical vapour deposition of zeolitic imidazolate framework thin films, Nature Mater. 15 (2016) 304–310, http://dx.doi.org/10.1038/nmat4509.

[10] S. Xie, Z. Zhou, X. Zhang, J. Fransaer, Cathodic deposition of MOF films: mechanism and applications, Chem. Soc. Rev. 52 (13) (2023) 4292–4312, http://dx.doi.org/10.1039/D3CS00131H.

[11] Z.-Z. Ma, Q.-H. Li, Z. Wang, Z.-G. Gu, J. Zhang, Electrically regulating nonlinear optical limiting of metal-organic framework film, Nature Commun. 13 (6347) (2022) 1–9, http://dx.doi.org/10.1038/s41467-022-34139-2.

[12] D.-J. Li, Q.-h. Li, Z.-R. Wang, Z.-Z. Ma, Z.-G. Gu, J. Zhang, Interpenetrated metal-porphyrinic framework for enhanced nonlinear optical limiting, J. Am. Chem. Soc. 143 (41) (2021) 17162–17169, http://dx.doi.org/10.1021/jacs.1c07803.

[13] R. Zhai, Y. Xiao, Z. Gu, J. Zhang, Tunable chiroptical application by encapsulating achiral lanthanide complexes into chiral MOF thin films, Nano Res. 15 (2) (2022) 1102–1108, http://dx.doi.org/10.1007/s12274-021-3610-x.

[14] F. Haase, P. Hirschle, R. Freund, S. Furukawa, Z. Ji, S. Wuttke, Beyond frameworks: Structuring reticular materials across nano-, meso-, and bulk regimes, Angew. Chem. Int. Edn 59 (50) (2020) 22350–22370, http://dx.doi.org/10.1002/anie.201914461.

[15] K. Sugiyama, K. Kiyokawa, H. Matsuoka, A. Itou, K. Hasegawa, K. Tsutsumi, Generation of non-equilibrium plasma at atmospheric pressure and application for chemical process, Thin Solid Films 316 (1) (1998) 117–122, http://dx.doi.org/10.1016/S0040-6090(98)00400-3.

[16] O. Goossens, E. Dekempeneer, D. Vangeneugden, R. Van de Leest, C. Leys, Application of atmospheric pressure dielectric barrier discharges in deposition, cleaning and activation, Surf. Coat. Technol. 142–144 (2001) 474–481, http://dx.doi.org/10.1016/S0257-8972(01)01140-9.

[17] J.M. Thiébaut, T. Belmonte, D. Chaleix, P. Choquet, G. Baravian, V. Puech, H. Michel, Comparison of surface cleaning by two atmospheric pressure discharges, Surf. Coat. Technol. 169–170 (2003) 186–189, http://dx.doi.org/10.1016/S0257-8972(03)00043-4.

[18] M. Noeske, J. Degenhardt, S. Strudthoff, U. Lommatzsch, Plasma jet treatment of five polymers at atmospheric pressure: surface modifications and the relevance for adhesion, Int. J. Adhes. Adhes. 24 (2) (2004) 171–177, http://dx.doi.org/10.1016/j.ijadhadh.2003.09.006.

[19] J.Y. Jeong, S.E. Babayan, V.J. Tu, J. Park, I. Henins, R.F. Hicks, G.S. Selwyn, Etching materials with an atmospheric-pressure plasma jet, Plasma Sources. Sci. Technol. 7 (3) (1998) 282, http://dx.doi.org/10.1088/0963-0252/7/3/005.

[20] M. Jasiński, J. Mizeraczyk, Z. Zakrzewski, T. Ohkubo, J.-S. Chang, CFC-11 destruction by microwave torch generated atmospheric-pressure nitrogen discharge, J. Phys. D: Appl. Phys. 35 (18) (2002) 2274, http://dx.doi.org/10.1088/0022-3727/35/18/308.

[21] R. Gholami, C.E. Stere, A. Goguet, C. Hardacre, Non-thermal-plasma-activated de-NOx catalysis, Philos. Trans. R. Soc. A 376 (2110) (2018) 20170054, http://dx.doi.org/10.1098/rsta.2017.0054.

[22] C. Tendero, C. Tixier, P. Tristant, J. Desmaison, P. Leprince, Atmospheric pressure plasmas: A review, Spectrochim. Acta B 61 (1) (2006) 2–30, http://dx.doi.org/10.1016/j.sab.2005.10.003.

[23] S. Xu, S. Chansai, C. Stere, B. Inceesungvorn, A. Goguet, K. Wangkawong, S.F.R. Taylor, N. Al-Janabi, C. Hardacre, P.A. Martin, X. Fan, Sustaining metal–organic frameworks for water–gas shift catalysis by non-thermal plasma, Nat. Catal. 2 (2019) 142–148, http://dx.doi.org/10.1038/s41929-018-0206-2.

[24] M. Sadakiyo, S. Yoshimaru, H. Kasai, K. Kato, M. Takata, M. Yamauchi, A new approach for the facile preparation of metal–organic framework composites directly contacting with metal nanoparticles through arc plasma deposition, Chem. Commun. 52 (54) (2016) 8385–8388, http://dx.doi.org/10.1039/C6CC02729F.

[25] J. Bae, J.-W. Jung, H.Y. Park, C.-H. Cho, J. Park, Oxygen plasma treatment of HKUST-1 for porosity retention upon exposure to moisture, Chem. Commun. 53 (89) (2017) 12100–12103, http://dx.doi.org/10.1039/C7CC05845D.

[26] J.B. Decoste, G.W. Peterson, M.W. Smith, C.A. Stone, C.R. Willis, Enhanced stability of Cu-BTC MOF via perfluorohexane plasma-enhanced chemical vapor deposition, J. Am. Chem. Soc. 134 (3) (2012) 1486–1489, http://dx.doi.org/10.1021/ja211182m.

[27] Z.-G. Gu, A. Pfriem, S. Hamsch, H. Breitwieser, J. Wohlgemuth, L. Heinke, H. Gliemann, C. Wöll, Transparent films of metal-organic frameworks for optical applications, Microporous Mesop. Mater. 211 (2015) 82–87, http://dx.doi.org/10.1016/j.micromeso.2015.02.048.

[28] S.S.-Y. Chui, S.M.-F. Lo, J.P.H. Charmant, A.G. Orpen, I.D. Williams, A chemically functionalizable nanoporous material [Cu3(TMA)2(H2O)3]n, Science 283 (5405) (1999) 1148–1150, http://dx.doi.org/10.1126/science.283.5405.1148.

[29] V.A. Milichko, S.V. Makarov, A.V. Yulin, A.V. Vinogradov, A.A. Krasilin, E. Ushakova, V.P. Dzyuba, E. Hey-Hawkins, E.A. Pidko, P.A. Belov, Van der Waals metal-organic framework as an excitonic material for advanced photonics, Adv. Mater. 29 (12) (2017) 1606034, http://dx.doi.org/10.1002/adma.201606034.

[30] K. Müller, K. Fink, L. Schöttner, M. Koenig, L. Heinke, C. Wöll, Defects as color centers: The apparent color of metal–organic frameworks containing Cu2+-based paddle-wheel units, ACS Appl. Mater. Interfaces 9 (42) (2017) 37463–37467, http://dx.doi.org/10.1021/acsami.7b12045.

[31] I.G. Koryakina, S.V. Bachinin, E.N. Gerasimova, M.V. Timofeeva, S.A. Shipilovskikh, A.S. Bukatin, A. Sakhatskii, A.S. Timin, V.A. Milichko, M.V. Zyuzin, Microfluidic synthesis of metal-organic framework crystals with surface defects for enhanced molecular loading, Chem. Eng. J. 452 (2023) 139450, http://dx.doi.org/10.1016/j.cej.2022.139450.

[32] A.S. Efimova, P.V. Alekseevskiy, M.V. Timofeeva, Y.A. Kenzhebayeva, A.O. Kuleshova, I.G. Koryakina, D.I. Pavlov, T.S. Sukhikh, A.S. Potapov, S.A. Shipilovskikh, N. Li, V.A. Milichko, Exfoliation of 2D metal-organic frameworks: toward advanced scalable materials for optical sensing, Small Methods 7 (11) (2023) 2300752, http://dx.doi.org/10.1002/smtd.202300752.

[33] P.V. Alekseevskiy, S. Rzhevskiy, V. Gilemkhanova, N.K. Kulachenkov, A. Sapianik, M. Barsukova, V.P. Fedin, V.A. Milichko, Flexible metal-organic framework for mechanical sub tbyte inch-2 data recording under ambient condition, Adv. Mater. Interfaces 8 (22) (2021) 2101196, http://dx.doi.org/10.1002/admi.202101196.

[34] N.K. Kulachenkov, D. Sun, Y.A. Mezenov, A.N. Yankin, S. Rzhevskiy, V. Dyachuk, A. Nominé, G. Medjahdi, E.A. Pidko, V.A. Milichko, Photochromic free MOF-based near-infrared optical switch, Angew. Chem. 132 (36) (2020) 15652–15656, http://dx.doi.org/10.1002/ange.202004293.

[35] C. Prestipino, L. Regli, J.G. Vitillo, F. Bonino, A. Damin, C. Lamberti, A. Zecchina, P.L. Solari, K.O. Kongshaug, S. Bordiga, Local structure of framework cu(II) in HKUST-1 metallorganic framework: spectroscopic characterization upon activation and interaction with adsorbates, Chem. Mater. 18 (5) (2006) 1337–1346, http://dx.doi.org/10.1021/cm052191g.

SUPPORTING INFORMATION

Non-Thermal Plasma Etching of MOF Thin Films in High Optical Quality

Pavel Alekseevskiy,[1] Maria Timofeeva,[1] Semyon Bachinin,[1] Cedric Noel,[2] Regis Peignier,[2] Pascal Boulet,[2] Thierry Belmonte,[2*] Valentin A. Milichko[1,2 **]

[1] School of Physics and Engineering, ITMO University, St. Petersburg, 197101, Russia

[2] Université de Lorraine, CNRS, IJL, F-54000 Nancy, France

*Email: thierry.belmonte@univ-lorraine.fr; v.milichko@metalab.ifmo.ru

OPTICAL CHARACTERIZATION

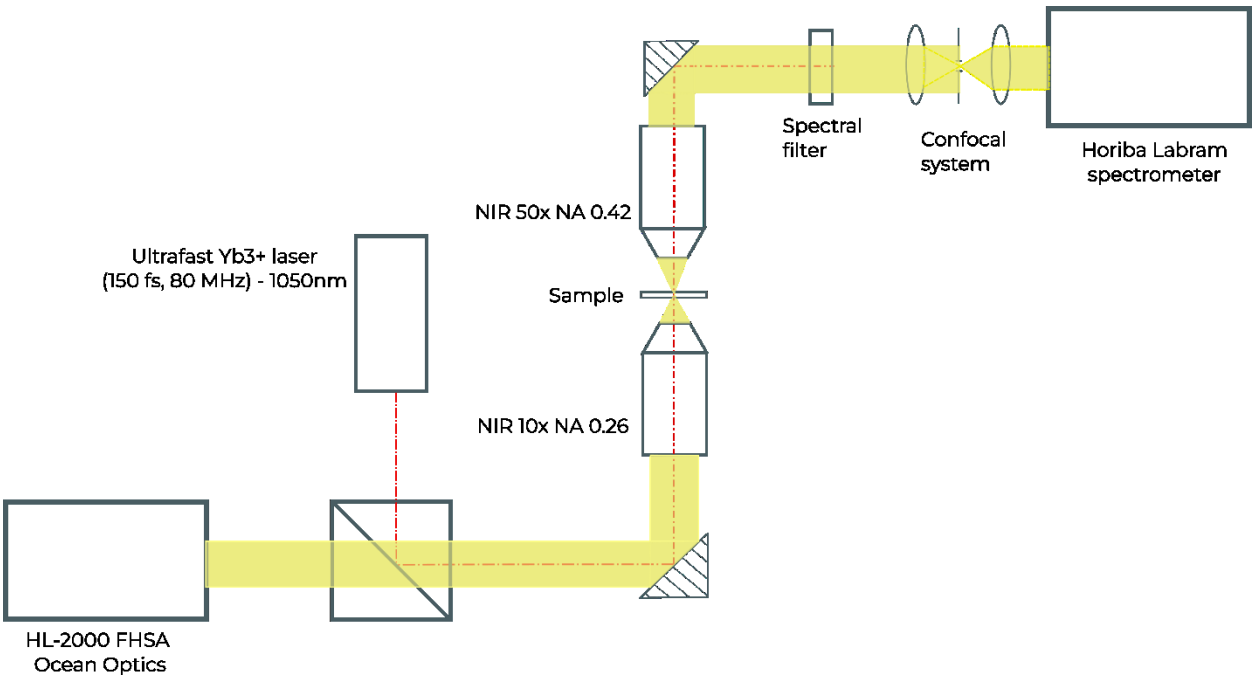

Figure S1. Scheme of the confocal optical setup used for sensing and characterization experiments.

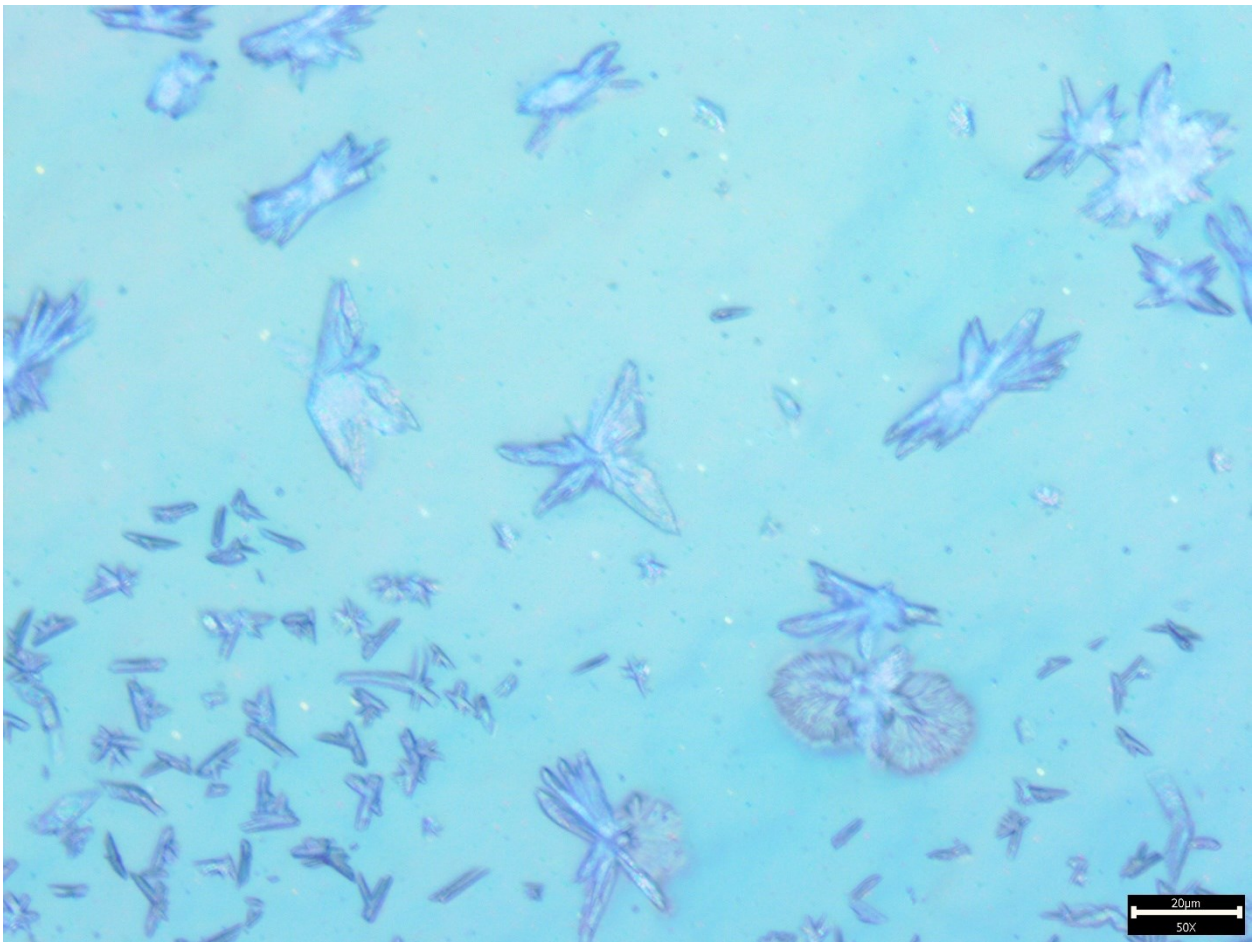

Figure S2. Optical image of the HKUST-1 TF before plasma etching (400 cycles, 50x magnification).

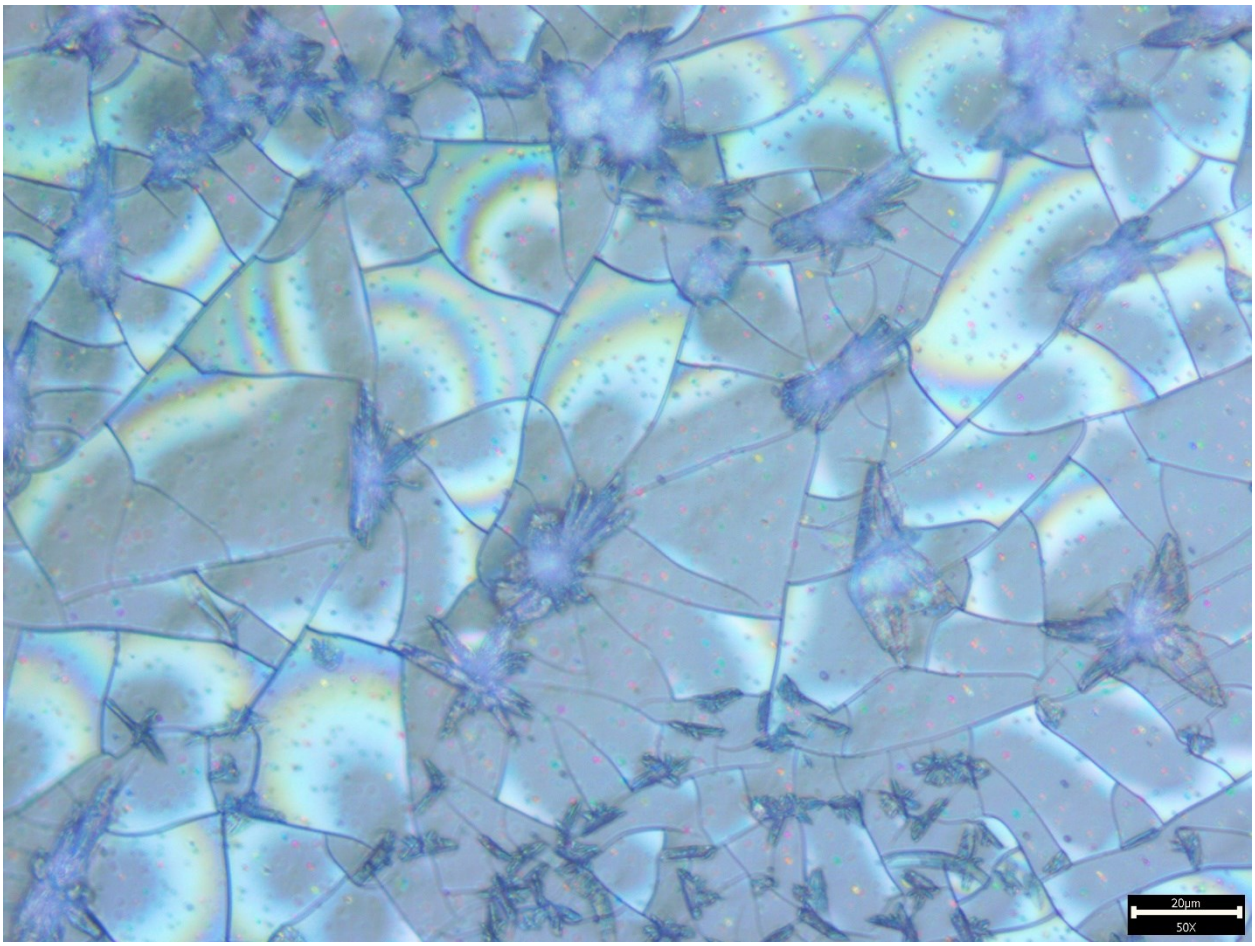

Figure S3. Optical image of the PESC HKUST-1 TF (400 cycles, 50x magnification, 3 min of PE treatment).

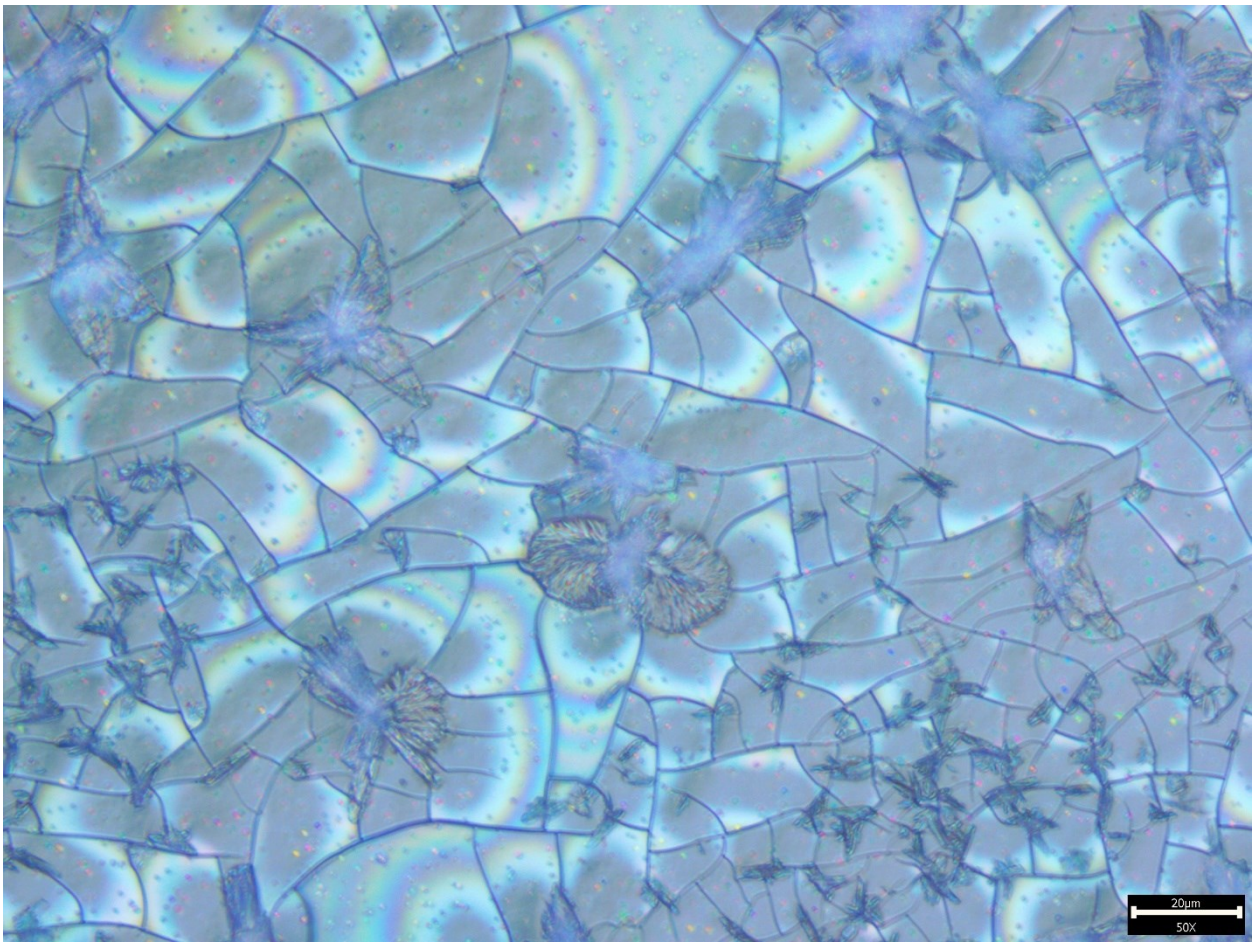

Figure S4. Optical image of the PESC HKUST-1 TF (400 cycles, 50x magnification, 5 min of PE treatment).

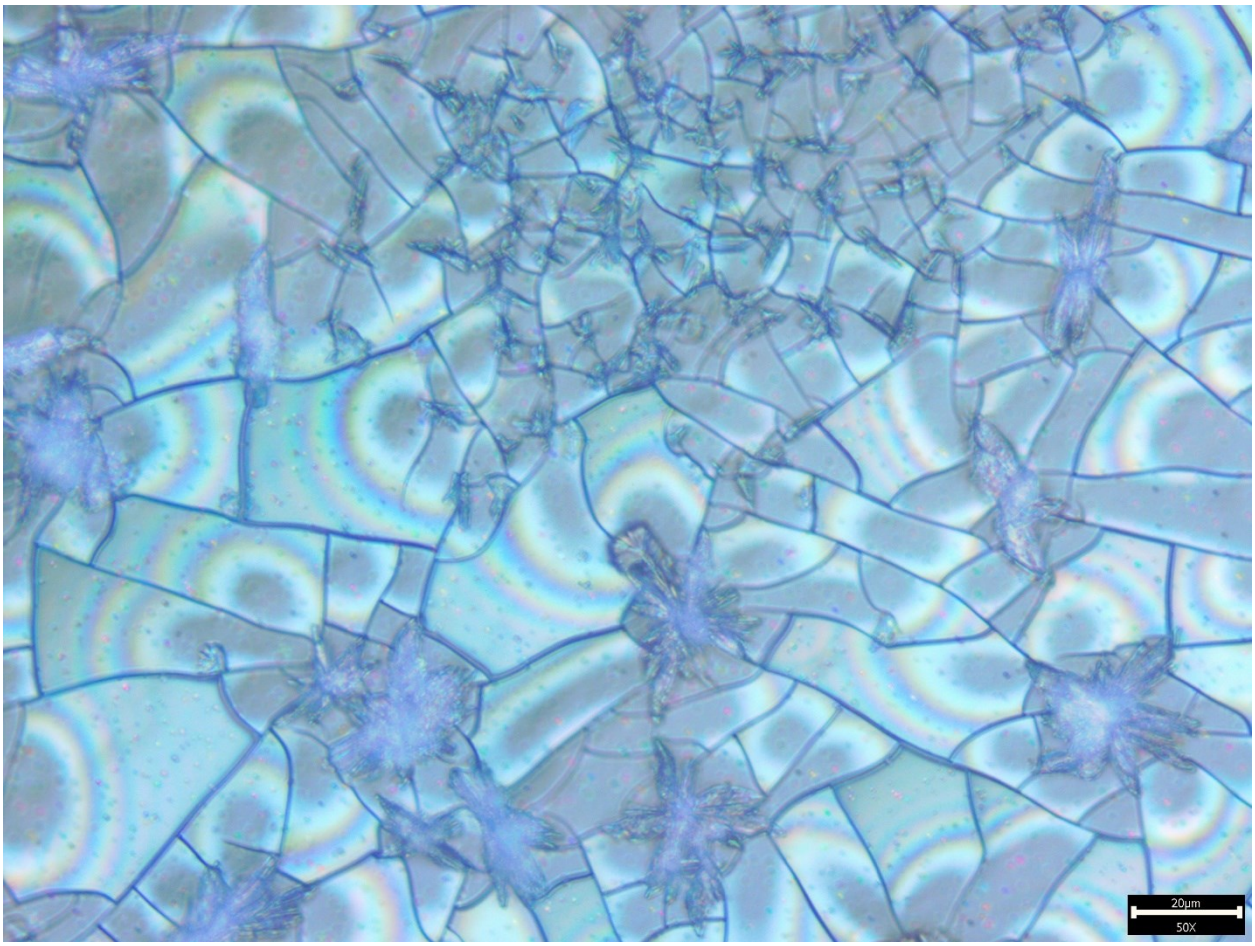

Figure S5. Optical image of the PESC HKUST-1 TF (400 cycles, 50x magnification, 7 min of PE treatment).

X-RAY DIFFRACTION ANALYSIS

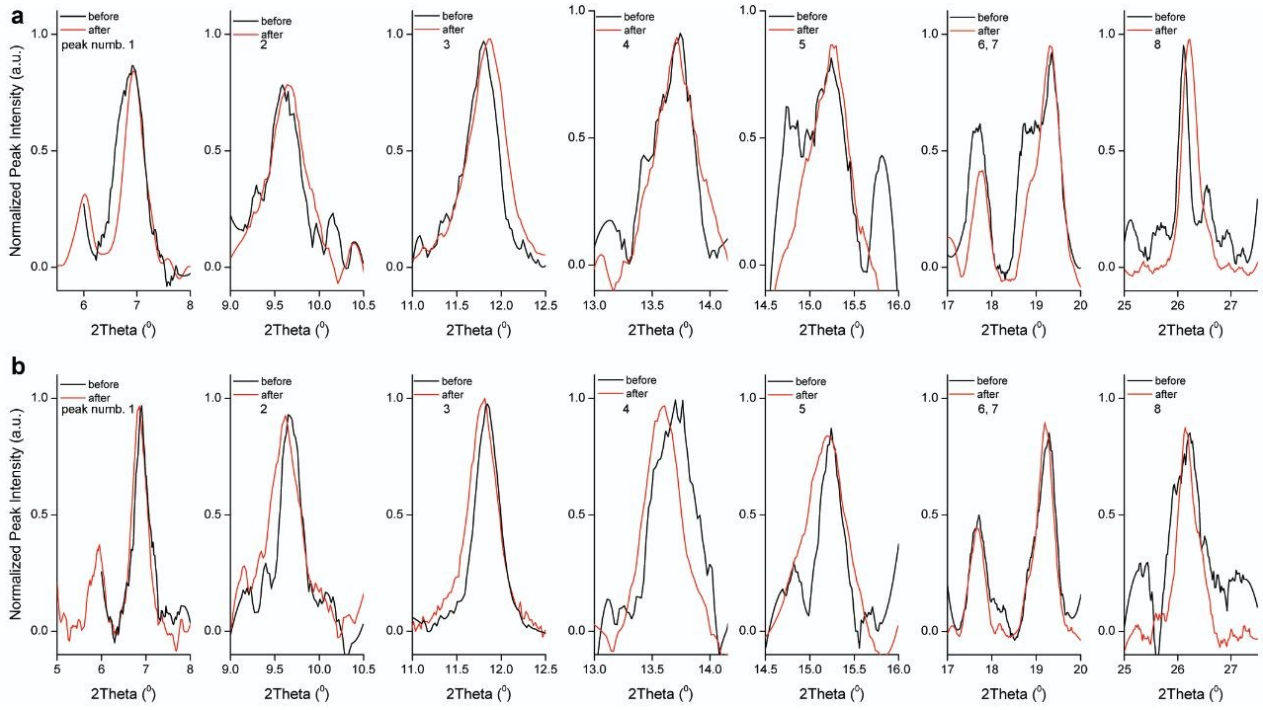

Figure S6. Comparison of the characteristic diffraction's peaks for each HKUST-1 TF: as-syntesized (black line) and PESC (red line), respectively. HKUST-1 TF (400 cycles (a)) and HKUST-1 TF (600 cycles (b)).

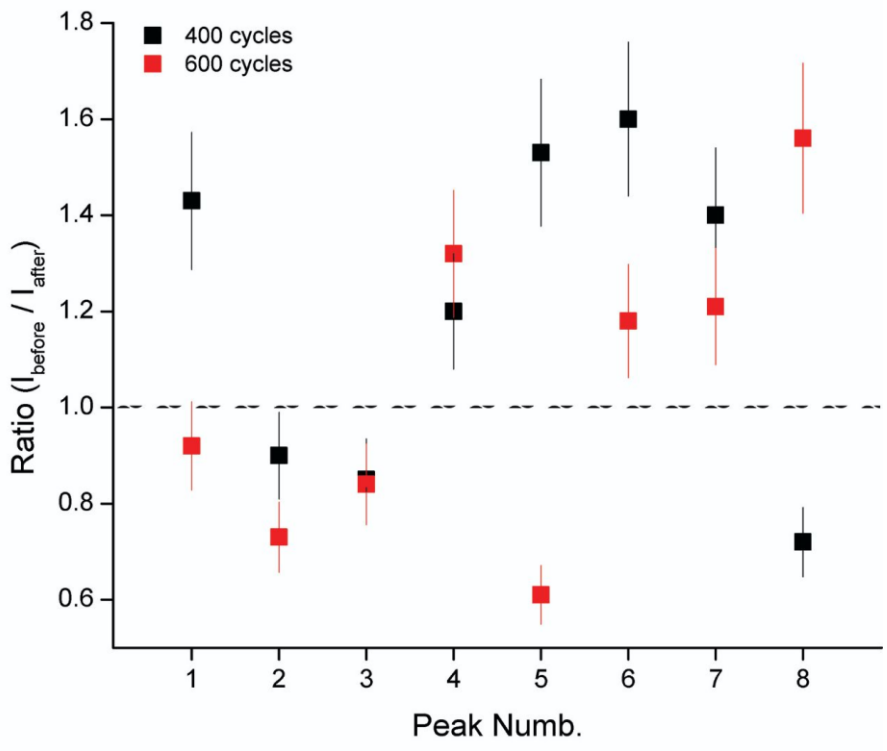

Figure S7. Comparison of the intensity ration of the FWHM diffraction's peaks of the HKUST-1 TF before and after plasma etching.

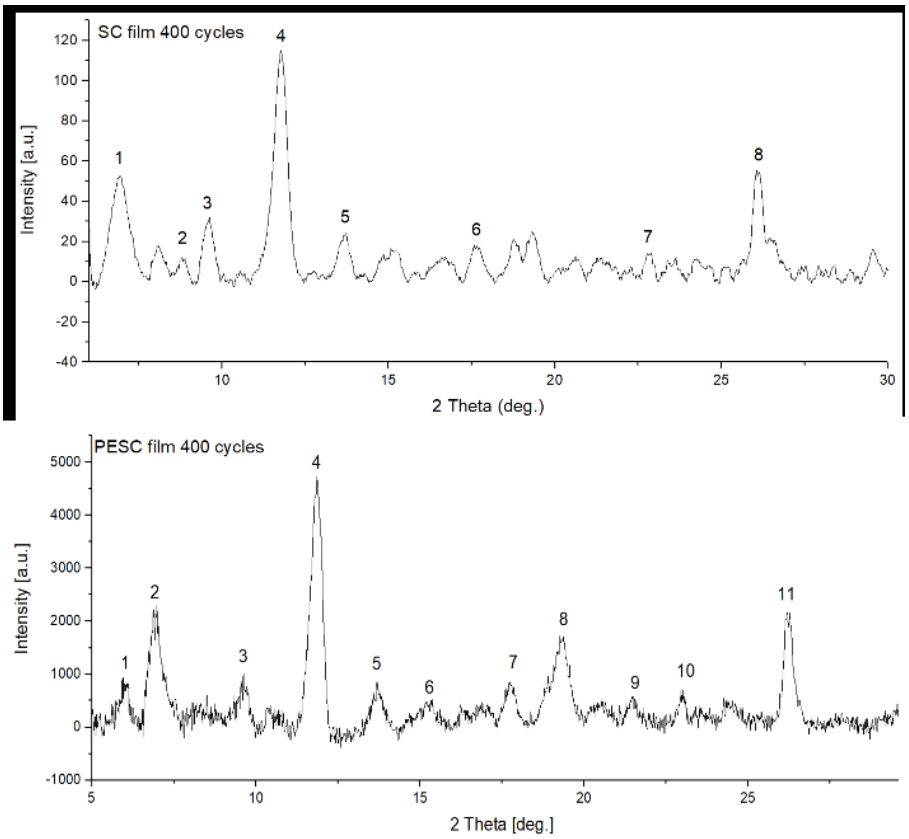

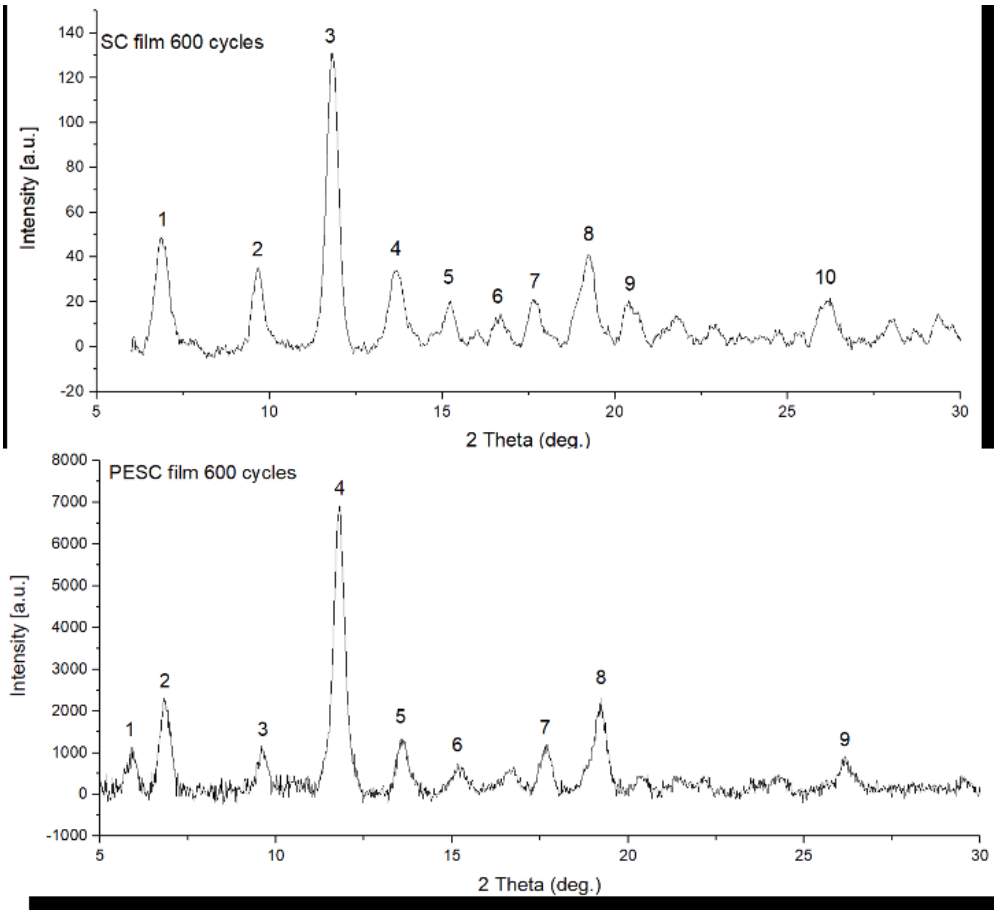

Figure S8. PXRD spectra of as-synthesized and PESC HKUST-1 TFs.

Figure S8 shows X-ray diffraction pattern of HKUST-1 thin films (produced in this study before and after PE). The formation of HKUST-1 was confirmed by the presence of the characteristic peaks in each XRD pattern [S1]. The broad peaks observed in each XRD pattern confirm that nano-crystallite films are produced. The appearance of narrow diffraction peaks after the PE (PESC HKUST-1 TF, 400 and 600 synthesis cycles) indicates an increase in the degree of crystallinity of the thin film. Using the Scherrer equation [S2] the average crystallite size for as-synthesized (400 and 600 synthesis cycles) and PESC HKUST-1 TFs (400 and 600 synthesis cycles) was estimated, as shown in Table S1 including the full width at half maximum (FWHM).

Table S1. As-synthesized HKUST-1 TF (400 and 600 cycles) and PESC HKUST-1 TF (400 and 600 cycles) crystallite sizes calculated by Scherrer Equation.

Peak	Angle (2 θ)	FWHM (2 θ)	Calculated crystallite size (nm)	Average crystallite size (nm)
As-synthesized HKUST-1 TF, 400 cycles				
1	6.9	0.5	14.5	27.5
2	8.9	0.2	48.1	
3	9.6	0.3	26.8	
4	11.8	0.5	17.4	
5	13.67	0.3	25.6	
6	17.6	0.3	26.8	
7	22.8	0.2	41.3	
8	26.1	0.4	19.7	
As-synthesized HKUST-1 TF, 600 cycles				
1	6.9	0.4	18.7	19.4
2	9.7	0.3	23.8	
3	11.8	0.4	20.3	
4	13.7	0.5	17.3	
5	15.2	0.3	23.0	
6	16.7	0.4	22.2	
7	17.7	0.4	21.7	
8	19.2	0.5	14.7	
9	20.5	0.5	17.1	
10	26.1	0.5	15.4	
PESC HKUST-1 TF, 400 cycles				
1	5.9	0.4	22.4	19.8
2	6.9	0.5	16.1	
3	9.6	0.4	20.7	
4	11.8	0.4	19.8	
5	13.7	0.4	22.4	
6	15.2	0.6	14.6	
7	17.7	0.4	19.9	
8	19.3	0.7	11.5	
9	21.5	0.5	17.9	

10	22.9	0.3	29.8	
11	26.2	0.4	23.2	
PESC HKUST-1 TF, 600 cycles				
1	5.9	0.3	25.0	21.6
2	6.9	0.3	23.0	
3	9.6	0.3	25.7	
4	11.8	0.4	20.3	
5	13.6	0.3	22.9	
6	15.2	0.4	19.7	
7	17.7	0.3	23.2	
8	19.2	0.5	17.4	
9	26.2	0.5	17.0	

ATOMIC FORCE MICROSCOPY

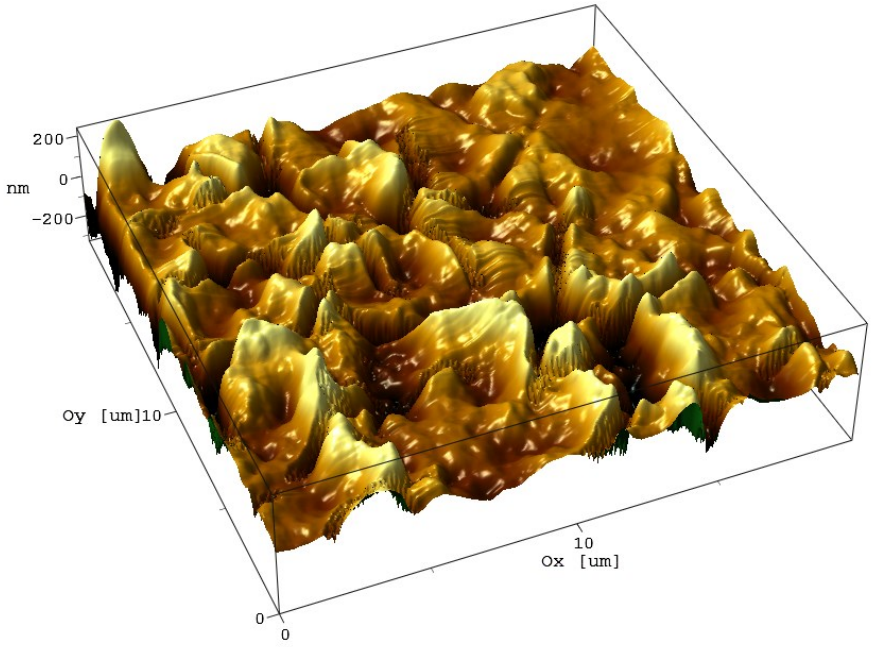

Figure S9. 3D plot of HKUST-1 TF surface before the plasma etching (Figure 5a).

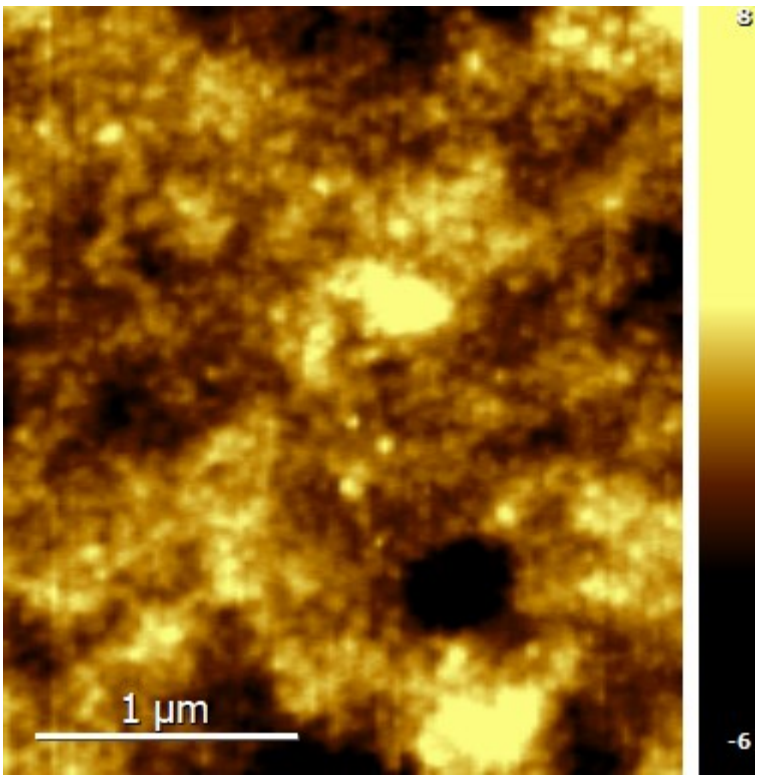

Figure S10. AFM scan of the PESC HKUST-1 TF surface (Z-bar in nm scale).

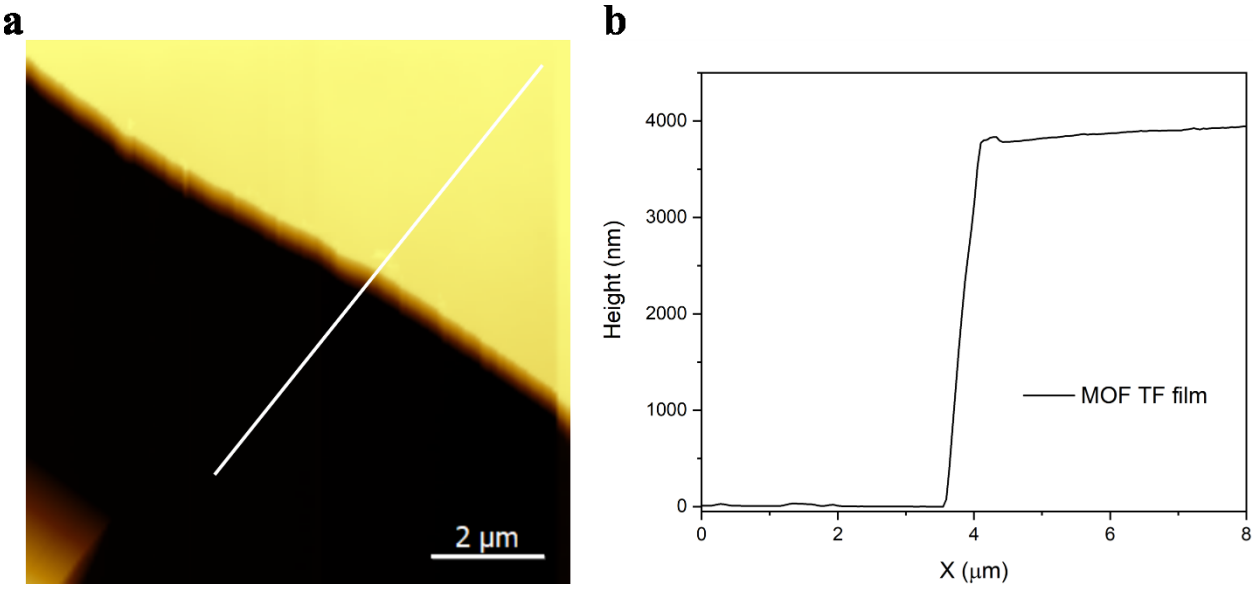

Figure S11. (a) AFM scan of the PESC HKUST-1 TF surface with (b) corresponding cross-section (white line).

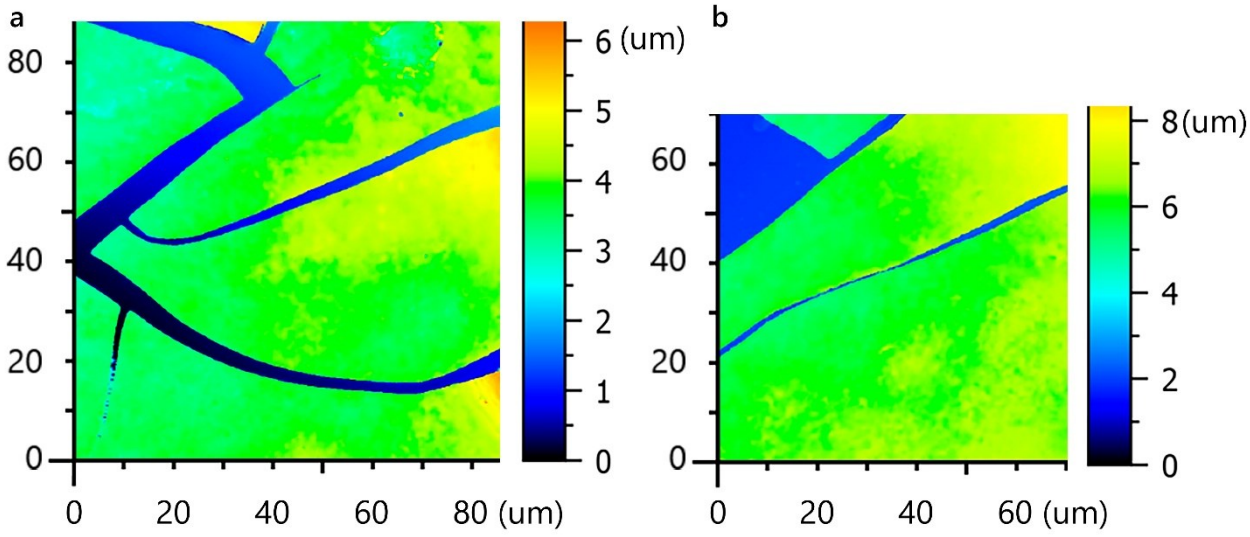

Figure S12. Optical profilometry of PESC HKUST-1 TF.

ENERGY DISPERSIVE X-RAY (EDX) and OSE ANALYSIS

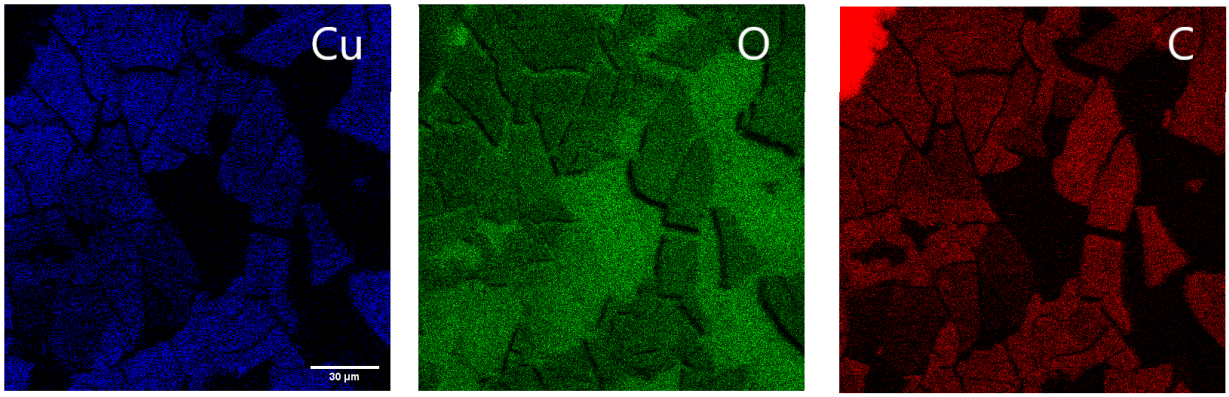

Figure S13. EDX mapping of the elements in PESC HKUST-1 TF.

As ions at atmospheric pressure do not gain enough energy to overcome the thresholds needed for sputtering, we assumed that the thin film is etched chemically. Optical emission spectroscopy, from 230 nm to 800 nm (Figure S14) shows the following emissions systems:

- NO-γ system ($A^2\Sigma^+ - X^2\Pi$)
- OH 3604 Å system ($A^2\Sigma^+ - X^2\Pi$)
- NH 3360 Å system ($A^2\Pi - X^3\Sigma^-$)
- N_2 second positif system (SPS) ($C^3\Pi_u - B^3\Pi_g$)
- Ar I and O I lines

No emissions of copper, carbon, or carbon-containing molecules were observed. The absence of these species from the film in the spectrum could be due to their lack of excitation.

Upon comparing this spectrum with a similar one [S3], the only discernible difference is the presence of NH emission lines. We propose that the etching mechanism of the HKUST-1 film proceeds through hydrogen abstraction via reaction with active nitrogen species from the discharge.

At this stage, we cannot definitively assert that oxygen is also etched from the film via NO formation, as NO emissions are present even without the film. Further investigations are now necessary to confirm and expand upon this scenario.

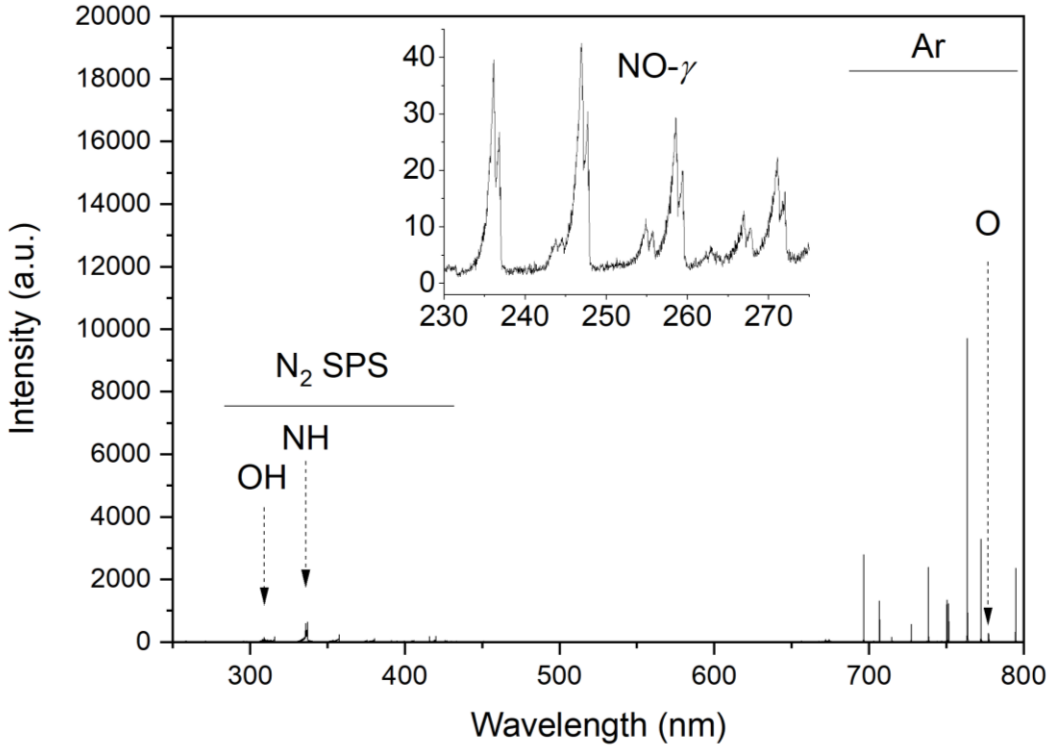

Figure S14. Optical emission spectrum of the argon plasma in air in contact with the HKUST-1 thin film.

SUPPLEMENTARY REFERENCES

[S1] Yakovenko, A. A., Reibenspies, J. H., Bhuvanesh, N. & Zhou, H.-C. Generation and applications of structure envelopes for porous metal–organic frameworks. J Appl Crystallogr 46, 346–353 (2013).

[S2] Saleh, T. A. Structural characterization of hybrid materials. in Polymer Hybrid Materials and Nanocomposites 213–240 (Elsevier, 2021). doi:10.1016/B978-0-12-813294-4.00005-4.

[S3] Rezaei, F., Gorbanev, Y., Chys, M., Nikiforov, A., Van Hulle, S. W., Cos, P., Bogaerts, A, De Geyter, N. Investigation of plasma-induced chemistry in organic solutions for enhanced electrospun PLA nanofibers. Plasma Process Polym 15(6), 1700226 (2018).